Morphology of binary blends of linear and branched polyethylene: composition and crystallization-temperature dependence

M. T. Conde Braña and U. W. Gedde*

Department of Polymer Technology, Royal Institute of Technology, S-10044 Stockholm, Sweden

(Received 21 January 1991; revised 12 July 1991; accepted 2 September 1991)

The morphology of binary mixtures of low-molar-mass linear polyethylene (L2.5: $M_w = 2500$, $M_w/M_n = 1.15$) and higher-molar-mass branched polyethylenes, with 0.5 mol% of butyl branches (BB0.5) or 1.5 mol% of ethyl branches (BE1.5), has been studied by differential scanning calorimetry, polarized light microscopy and transmission electron microscopy. A progressive change from curved to straight lamellae and a strong decrease in average amorphous thickness is observed with increasing content of the linear polymer. Data obtained by model calculations of the average amorphous thickness assuming complete co-crystallization of the linear and branched polymers show good correspondence with the experimental data obtained for blends of L2.5 and BE1.5 except for the blend consisting of 80% of L2.5 but a pronounced deviation for blends of L2.5 and BB0.5. For the majority of the blends of L2.5 and BE1.5 there is a good agreement between calorimetric crystallinity and crystallinity determined by transmission electron microscopy, which indicates co-crystallization of the components. There is, however, significant deviation between the two crystallinity values for all blends of L2.5 and BB0.5, and for the blend of L2.5 and BE1.5 with 80% of L2.5, which can be explained by partial segregation of L2.5.

(Keywords: binary blends; linear polyethylene; branched polyethylene; morphology; co-crystallization; transmission electron microscopy)

INTRODUCTION

The morphology of blends of linear and branched polyethylene (PE) has received considerable attention in recent years[1–9]. Unquestionably the two components in binary mixtures of linear and high-pressure branched PE are essentially incompatible in the solid state[1–3]. Blends of linear PE and low-pressure branched PE have been studied by several authors, and their conclusions are very different, although their studies have concerned similar polymers of relatively high molar mass with medium to high polydispersity and with the branched polymer containing 1.4–1.8 mol% of ethyl groups[4–6]. Hu *et al.*[4] and Edwards[5] presented evidence obtained by differential scanning calorimetry (d.s.c.), wide- and small-angle X-ray diffraction (WAXS and SAXS) and Raman spectroscopy in support of co-crystallization of linear and branched PE.

Contrary to this view, Norton and Keller[6] reported data obtained by d.s.c., polarized light microscopy and transmission electron microscopy (TEM) establishing predominantly segregation of linear and branched (1.4 mol% of ethyl groups) PE components in a 50/50 blend of commercial high-density polyethylene (HDPE) and linear, low-density polyethylene (LLDPE) crystallized at different constant temperatures between 394 and 403 K. The linear polymer crystallized first under isothermal conditions, forming regular-shaped sheets in a spherulitic morphology, whereas the branched polymers crystallized at a later stage during the rapid cooling in finer, S-shaped lamellae located between the stacks of dominant lamellae. Some, limited co-crystallization was, however, indicated in samples crystallized close to 394 K. The quenched samples exhibited less pronounced segregation according to d.s.c.

We have recently presented papers[7–9] dealing with the morphology and crystallization kinetics of binary mixtures of a low-molar-mass linear PE fraction ($M_w = 2500$, $M_w/M_n = 1.15$) and higher-molar-mass branched PE with a higher degree of polydispersity. TEM work[8] on chlorosulphonated sections clearly confirmed that co-crystallization occurred between the linear and branched components. The uniform crystalline and amorphous lamellar structure and the absence of white, unstained domains was the major evidence in support of co-crystallization[8]. Unstained domains are indicative of the presence of segregated, low-molar-mass polymer. The amorphous thickness proved to be the most sensitive morphological parameter: from being almost 15 nm in one of the pure branched polymers (1.3 mol% of ethyl groups) it decreased to near 6 nm in the 50/50 blend.

The isothermal crystal growth rate of binary mixtures of the low-molar-mass linear polyethylene and high-molar-mass ethyl-branched (1.5 mol%) polyethylene (BPE) was found to increase strongly with increasing content of the linear polymer[9]. The growth-rate data were treated according to the Hoffman–Miller theory assuming that the linear growth rate was determined by

*To whom correspondence should be addressed

0032-3861/92/153123-14

the longest linear chain segments of the branched polymer. The low-molar-mass polymer affected only the pre-exponential factor (G_0) related to short-distance diffusion of the crystallizable segments; G_0 increased by more than one order of magnitude when the content of L2.5 was increased from 0 to 80%. Additional data obtained by polarized light microscopy and d.s.c. indicated that crystallization involved first only a minor fraction, about 10% of the branched polymer, consisting of relatively long linear chain segments. At a later stage BPE chain segments of lower perfection and linear polymer species co-crystallized[9]. The second mechanism involved most of the material. This process occurred at a rate comparable with that associated with the first mechanism and controlled the morphology as revealed by polarized light microscopy.

The present paper is a follow-up of the previous work[7–9] on blends of low-molar-mass linear PE and higher-molar-mass branched PE and presents data obtained by d.s.c., polarized light microscopy and TEM. In this paper, attention is focused on the effect of crystallization temperature and blend composition on the following morphological features: (i) crystal and amorphous thickness distribution; (ii) co-crystallization or separate crystallization; (iii) shape of crystal lamellae; (iv) higher-order organization; and (v) melting behaviour.

EXPERIMENTAL

Binary mixtures of different compositions of a linear PE sharp fraction ($M_w = 2500$, $M_w/M_n = 1.15$), referred to as L2.5, purchased from Polymer Laboratories Ltd, UK, and two different branched PE fractions were prepared by a solution mixing technique previously described[8]. The branched PE fractions were prepared from experimental PE grades produced by Neste Polyeten AB, Sweden, and are referred to as BE1.5 ($M_n = 27\,000$, $M_w = 166\,000$, 1.5 mol% of ethyl branches) and BB0.5 ($M_n = 20\,000$, $M_w = 290\,000$, 0.5 mol% of butyl branches). The average molar mass and chain branching data were obtained by size exclusion chromatography and ^{13}C nuclear magnetic resonance spectroscopy[8].

The blends were thermally treated in a nitrogen atmosphere in a temperature-calibrated Perkin–Elmer DSC-7. The samples were melted in the d.s.c. apparatus at 440 K for 5 min, cooled at a rate of 80 K min^{-1} to the crystallization temperature, kept at this temperature for a specified period of time and finally cooled to room temperature at 80 K min^{-1}. Each blend was crystallized at two different temperatures and times, the latter given within brackets: 392.2 K (12 h) and 396.2 K (24 h) for L2.5/BB0.5 and 387.2 K (0.7 h) and 394.2 K (24 h) for L2.5/BE1.5.

The melting endotherms of all blends were recorded by d.s.c. at a heating rate of 10 K min^{-1}. The recorded values of heat of fusion were transformed into mass crystallinity, w_c(d.s.c.), using the total enthalpy method[10], equation (1), considering 293 kJ kg^{-1} (ref. 11) as the heat of fusion for 100% crystalline polymer at the equilibrium melting point (418.1 K[12]):

$$w_c\,(\text{d.s.c.}) = \Delta h\left(293 - \int_{T_1}^{418.1} (c_{pa} - c_{pc})\,dT\right)^{-1} \quad (1)$$

where Δh is the measured heat of melting, T_1 is a temperature below the melting range, and c_{pa} and c_{pc} are the specific heats of the amorphous and crystalline components, respectively. The data of Wunderlich and Baur[13] for c_{pa} and c_{pc} have been used.

The morphology was revealed by polarized light microscopy (Leitz Ortholux POL BK II equipped with crossed polarizers and a temperature-calibrated Mettler Hot Stage FP 82; all the observations were made at the crystallization temperature) and by TEM using a JEOL JEM 100 B electron microscope. The samples for TEM analysis were treated according to the method developed by either Kanig[14] or Olley and Bassett[15]. The experimental details of the Kanig treatment, chlorosulphonation and staining with uranyl acetate, have been presented in a previous paper[8]. The 50 nm thick sections were examined in the electron microscope. Shrinkage of the sections may take place when they are exposed to the electron beam even at low intensities[16]. Care was taken to use as low beam intensities as possible. Different parts of the samples were examined in order to reveal any variation in morphology.

The details of the analysis of the TEM micrographs have already been presented in a previous paper[8] but are repeated here. The thicknesses of crystals and amorphous layers were measured on magnified images of the negatives. The crystal lamellae and amorphous layers included in the analyses were selected by the intercept method, i.e. only those crossed by one of the introduced lines were chosen. These lines were always parallel and the line spacing was 300 nm. The accuracy of each measurement (reading) is 1 nm. Care was taken to ensure that only those crystal lamellae parallel to the electron beam were evaluated, by counting only the crystals and amorphous layers appearing with maximum sharp boundaries. The thickness of the boundary region ('grey zone') of the selected crystals is about 1 nm and the crystal thickness in the analysis is defined as the sum of the thickness of the white, unstained zone and one 'grey zone'. About 300 crystal and 300 amorphous interlayers were measured in each sample.

A few of the samples were etched for 20 h at 298 K under agitation in a 0.7% (w/w) solution of $KMnO_4$ in a (2/1) mixture of concentrated sulphuric acid (98%) and dry orthophosphoric acid (99%) according to the technique developed by Olley and Bassett[15]. The samples were subsequently washed, replicated in two stages using cellulose acetate for the first impression, shadowed with Au/Pd in a vacuum evaporator, coated with carbon and examined in the transmission electron microscope.

RESULTS AND DISCUSSION

The melting endotherms obtained by d.s.c. exhibit either two or three distinct peaks. The peak temperatures and their relative sizes are given in *Table 1*. The low-temperature peak is always associated with the material crystallizing in the cooling phase. It is always a mixture of low-melting-point linear and branched components. Three melting peaks are indicative of the formation of two different types of crystals at the isothermal crystallization temperature, i.e. 'isothermal' segregation. The temperature of the middle melting peak corresponds almost exactly to the melting point of pure L2.5.

The blends of L2.5 and BE1.5 displayed only two melting peaks except for the blend with 80% of L2.5, which displayed a weak, double, high-temperature peak after crystallization at 387.2 K. The crystallization at

Table 1 Thermal analysis data for blends

Sample[a]		T_c (K)[b]	Melting peak temperature (K) Relative peak size[c]			Δh_{tot} (kJ kg^{-1})[d]
L2.5/BE1.5	(0)	387.2	383.9 (0.52)		398.5 (0.48)	117
	(0.2)		388.7 (0.49)		399.9 (0.51)	141
	(0.4)		390.3 (0.46)		399.6 (0.54)	164
	(0.6)		389.8 (0.30)		400.4 (0.70)	193
	(0.8)		389.1 (0.20)	397.2[e]	399.3 (0.80)	211
	(1)		389.0 (0.10)	397.5 (0.90)		253
L2.5/BE1.5	(0)	394.2	389.0 (0.68)		403.9 (0.32)	114
	(0.2)		392.4 (0.74)		404.3 (0.26)	144
	(0.4)		393.9 (0.82)		403.0 (0.18)	170
	(0.6)		397.5 (0.88)		403.5 (0.12)	182
	(0.8)		398.2 (0.94)		403.1 (0.06)	217
L2.5/BB0.5	(0)	392.2	385.0 (0.29)		405.0 (0.71)	182
	(0.2)		393.0 (0.35)		404.5 (0.65)	196
	(0.4)		394.2 (0.37)		404.5 (0.63)	199
	(0.6)		394.0 (0.39)	397.8 (0.21)	403.6 (0.40)	223
	(0.8)		394.9 (0.42)	398.9 (0.39)	403.1 (0.19)	240
L2.5/BB0.5	(0)	396.2	390.6 (0.30)		407.2 (0.70)	173
	(0.2)		395.2 (0.55)		406.5 (0.45)	208
	(0.4)		396.5 (0.58)		405.4 (0.42)	205
	(0.6)		397.4 (0.72)		404.7 (0.28)	217
	(0.8)		397.8 (0.90)		404.0 (0.10)	243

[a]Mass content of L2.5 given within parentheses
[b]Crystallization temperature
[c]Relative peak size given within parentheses
[d]Total endothermic heat of melting
[e]Only a weak shoulder appeared; peak area included in higher-temperature peak

Table 2 Supermolecular structures[a] as revealed by polarized light microscopy

Constituents	T_c (K)[b]	Mass content of L2.5					
		0	0.2	0.4	0.6	0.8	1
L2.5/BE1.5	387.2	BS (1.4)	BS (2.3)	BS (2.9)	BS (4.6)	A	A
	394.2	NBS	NBS + A	A	A	A	A
L2.5/BB0.5	392.1	BS (1.6)	BS (2.5)	BS (3.1)	BS (4.1)	A	A
	396.1	BS (3.4)	BS (4.5)	BS (8.3)	NBS + A	A	A

[a]Abbreviation for structures: BS, banded spherulites (value in μm for band spacing given within parentheses); NBS, non-banded spherulites; A, axialites
[b]Crystallization temperature

387.2 K included most of both components in the blends studied, whereas at 394.2 K only a minor part of BE1.5 crystallized and the rest of BE1.5 and L2.5 crystallized during cooling.

Blends containing 60% or more of L2.5 and BB0.5 exhibited three melting peaks indicative of segregation when crystallized at 392.2 K. The low-temperature peak formed on quenching consisted of a mixture of predominantly L2.5 and to a lesser extent BB0.5. The blends crystallized at 392.2 K consisting of 40% or less of L2.5 displayed only two melting peaks. The d.s.c. data thus indicated that co-crystals were formed in the isothermal phase. Crystallization at 396.2 K involved only a part, about 70%, of BB0.5. The remainder of the BB0.5 and the L2.5 crystallized during cooling, resulting in a unimodal, low-temperature melting peak.

Polarized light microscopy showed that the morphology sensitively reflects the composition of the blends and the crystallization temperature (*Table 2*). The branched polymers displayed banded spherulites whereas L2.5 exhibited large sheaves (axialites). There was a monotonic increase in band spacing with increasing content of L2.5 until suddenly the banded spherulitic morphology was replaced either by non-banded spherulites or by axialites. This occurred at 60–80% of L2.5 for the samples crystallized at the lower temperatures, 392.2 K (L2.5/BB0.5) and 387.2 K (L2.5/BE1.5). At the higher crystallization temperatures, the morphology was also dominantly axialitic in blends with a lower content of L2.5.

Figures 1–4 present transmission electron micrographs of representative parts of the chlorosulphonated sections of the studied samples. The crystal lamellae appear white and the amorphous component dark. Crystals with sharp

contrast have their fold surfaces parallel to the direction of viewing, the latter being along [u v 0]. The location of the sections should be random with respect to the centres of the spherulites (axialites). From simple geometrical considerations it can be deduced that the average distance between the section and the spherulite centre should be $R/\sqrt{3}$, where R is the radius of the spherulites. It is well established that [0 1 0] is parallel to the radius of a mature spherulite[17]. Hence, sharply appearing crystal lamellae are dominantly viewed along [0 1 0]: 40% of the surface is within a 20° angle from [0 1 0] and 60% within a 30° angle from [0 1 0]. On low-level magnifications (not shown in this paper), it was possible to identify spherulites of sizes corresponding to those obtained by polarized light microscopy. Roof-shaped and S-shaped lamellae appeared mostly in the 'viewing' centre of the spherulites, thus when viewed along [0 1 0]. A more detailed discussion about the orientation of the roof-shaped lamellae is given later in the paper.

Consider blends of L2.5 and BE1.5, illustrated in *Figures 1* and *2*. The blends with 0% and 20% of L2.5 display long S-shaped lamellae surrounding significantly shorter lamellae of the same or lower thickness after crystallization at 387.2 K (*Figures 1a* and *1b*). The morphology of the same blends crystallized at 394.2 K is characterized by straight or slightly curved dominant lamellae (*Figures 2a* and *2b*). The S shape of these lamellae is more pronounced for pure BE1.5 than for the blend with 20% of L2.5. A general feature of these samples is also the presence of large domains of only thin S-shaped short lamellae. The contrast of these thin lamellae is for some unknown reason relatively low. A substantial change in the morphology occurs in the blend consisting of 40% of L2.5 (*Figures 1c* and *2c*). The lamellae in these samples are dominantly short, straight or slightly curved and more occasionally roof-ridge-shaped. The blend crystallized at 394.2 K shows also a few long, straight lamellae, in addition to the roof-ridge sheets (*Figure 2c*). For the blends containing 60% or more of L2.5, the lamellae are straight and occasionally roof-ridge-shaped (*Figures 1d*, *1e*, *2d* and *2e*). The number of lamellae per stack increased substantially compared with the blends with a lower content of L2.5. A monotonic decrease in thickness of the amorphous interlayers with increasing content of L2.5 is also strikingly apparent in the micrographs.

Next, consider blends of L2.5 and BB0.5, shown in *Figures 3* and *4*. Curved or S-shaped lamellae are typical of BB0.5 (i.e. blend with 0% of L2.5) at both crystallization temperatures (*Figures 3a* and *4a*). Additional stacks of straight, short and equally thick lamellae located between the long C- or S-shaped lamellae are observed in BB0.5 crystallized at 396.2 K in contrast to the more uniform structure revealed in BB0.5 after crystallization at 392.2 K. The blend consisting of 20% of L2.5 exhibits long and slightly curved lamellae surrounded by short, equally thick or thinner lamellae oriented at some angle with respect to the dominant lamellae (*Figures 3b* and *4b*). The blends of 40% and 60% of L2.5 exhibit both straight and slightly curved (C-shaped) lamellae and, after being crystallized at 396 K, also occasional roof-ridges (*Figures 3c*, *3d*, *4c* and *4d*). The blends of 80% of L2.5 contain only straight and tightly packed lamellae forming large stacks with a great many crystal lamellae (*Figures 3e* and *4e*).

Figure 5 shows transmission electron micrographs of two of the blends after they had been etched by potassium permanganate/sulphuric acid/phosphoric acid. They have features resembling those shown by the chlorosulphonated samples (*Figures 1–4*). The blend L2.5/BE1.5 (0.2/0.8) crystallized at 394.2 K, shown in *Figure 5a*, exhibits a less well organized structure with pronounced curved, S-shaped lamellae. It is also possible to make a distinction between dominant and subsidiary lamellae in this sample. The other sample shown in *Figures 5b* and *5c*, L2.5/BE1.5 (0.8/0.2) crystallized at 387.2 K, is more well organized with long and straight lamellae forming large stacks. Roof-shaped crystals occur occasionally in this sample. In a few cases (one example is shown in *Figure 5c*) it was possible to obtain a view from the top of the lamellae, i.e. along [0 0 1]. The faceted crystals displayed both {1 1 0} and (100) lateral surfaces.

An interesting comparison can be made between the crystallinity data obtained respectively by d.s.c. (equation (1)) and TEM (equation (2)):

$$w_c(\mathrm{TEM}) = \frac{\langle L_c \rangle \rho_c}{\langle L_c \rangle \rho_c + \langle L_a \rangle \rho_a} \qquad (2)$$

where $\langle L_c \rangle$ is the mass-average crystal thickness ($\sum N_i L_{ci}^2 / \sum N_i L_{ci}$), $\langle L_a \rangle$ is the mass-average amorphous layer thickness ($\sum N_i L_{ai}^2 / \sum N_i L_{ai}$), and ρ_c and ρ_a are the densities of the crystalline and amorphous components, respectively. Values for ρ_c and ρ_a are taken from ref. 18. *Figure 6* presents the two sets of data; the agreement is good for blends of L2.5 and BE1.5 except for the blend containing 80% of L2.5. The discrepancy is significant for blends of L2.5 and BB0.5. The crystallinity data obtained by TEM are always lower than those obtained by d.s.c. This deviation is most probably due to partial segregation of L2.5. It is known from previous work[8] that crystal lamellae of segregated L2.5 are not revealed by TEM of chlorosulphonated sections. If such segregated material exists, the corresponding crystals are not included in the numerical analysis of the TEM micrographs, and hence the crystallinity is underestimated by TEM. The fraction of segregated material of L2.5 (w_{segr}) is calculated by equation (3) under the assumption that the difference in crystallinity determined by the two methods is entirely due to the presence of segregated L2.5:

$$w_{segr} = \frac{w_c(\mathrm{d.s.c.}) - w_c(\mathrm{TEM})}{w_{L2.5}[w_{cL2.5} - w_c(\mathrm{TEM})]} \qquad (3)$$

where $w_{L2.5}$ is the content of L2.5 in the blend and $w_{cL2.5}$ is the crystallinity of pure L2.5, which is set to 0.90. *Figure 7* demonstrates that the fraction of segregated L2.5 is very substantial in the blends of L2.5 and BB0.5. D.s.c. showed no segregation between linear and branched PE in these blends; only two melting peaks were observed (*Table 1*). The TEM data indicate, however, that a substantial fraction of L2.5 is segregated and that the unimodal, low-temperature peak must be due to overlapping but separate melting peaks. The other series of blends, L2.5/BE1.5, exhibited predominantly co-crystals except for the blend containing 80% of L2.5.

Figures 8 and *9* present typical histograms representing the amorphous layer thickness distribution for two series of blends. The distribution is relatively broad for the pure branched polymers. The introduction of L2.5 makes the distributions gradually more narrow and shifted towards

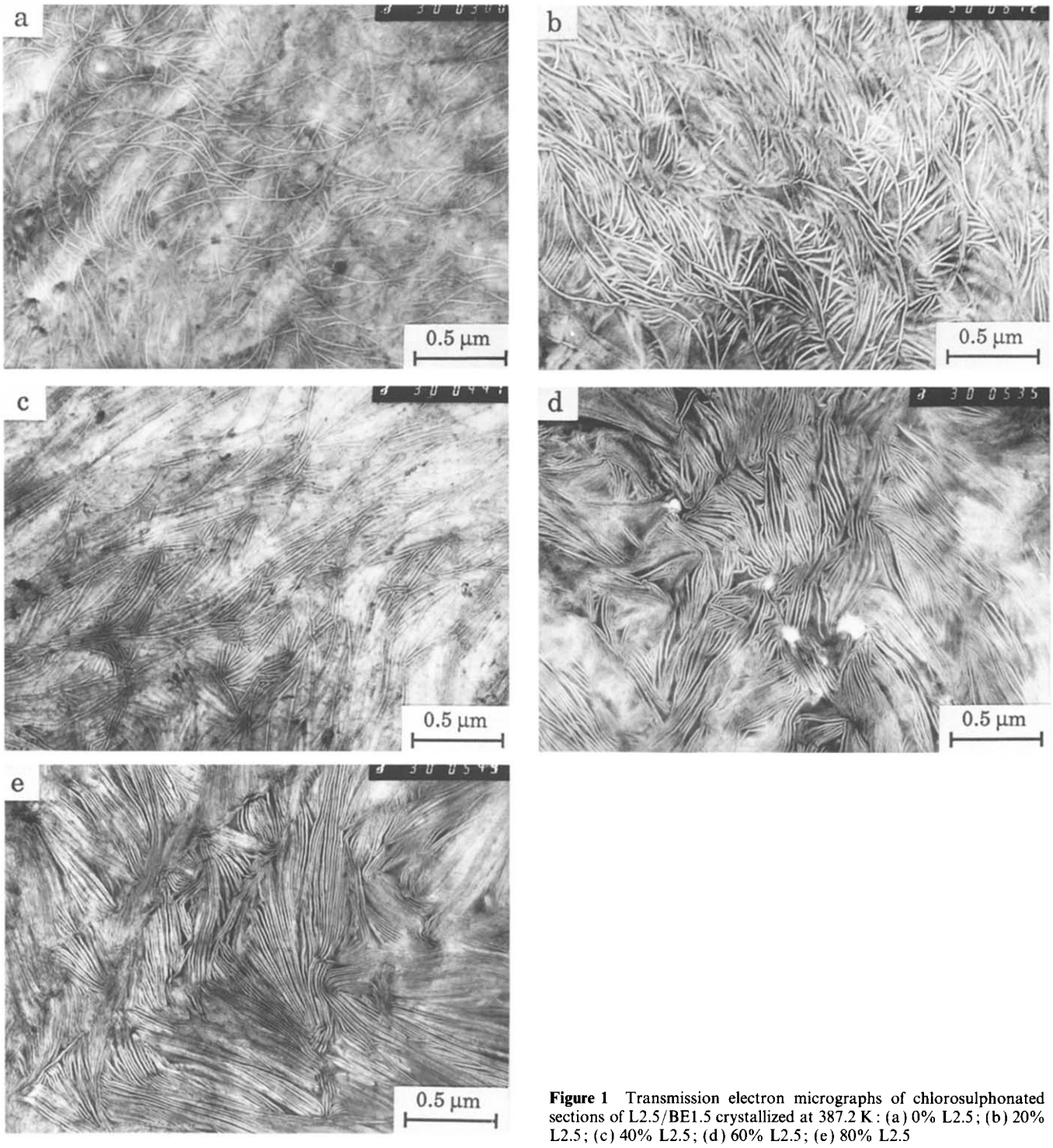

Figure 1 Transmission electron micrographs of chlorosulphonated sections of L2.5/BE1.5 crystallized at 387.2 K: (a) 0% L2.5; (b) 20% L2.5; (c) 40% L2.5; (d) 60% L2.5; (e) 80% L2.5

lower thickness values. All distributions appear to be unimodal. The shift of the distributions towards lower thickness values is more pronounced in L2.5/BE1.5 than in L2.5/BB0.5.

The data for the mass-average amorphous thickness ($\langle L_a \rangle$) plotted as a function of the mass content of L2.5 are compared in *Figure 10* with results from a model calculation of the amorphous thickness. The first assumption made here is that the nature of the amorphous segments of the branched polymer is not affected by the introduction of L2.5, i.e. the probability for tight chain folding (f) and the average volume (V_0) occupied by each random amorphous segment are independent of the local composition, i.e. mass content of L2.5 ($w_{L2.5}$). It is also assumed that L2.5 contributes to the amorphous phase by 10% of its total volume, also in this case independent of composition. The following equation is obtained under these assumptions:

$$\langle L_a \rangle = (1-f)N_{e0}(\cos\theta)V_0 \times \left(\frac{(1-w_{L2.5})w_{cBPE}}{(1-w_{L2.5})w_{cBPE} + w_{L2.5}w_{cL2.5}}\right) + \frac{0.1M_w(\cos\theta)\rho_c L_{rep}}{M_{rep}\rho_a} \times \left(\frac{w_{L2.5}w_{cL2.5}}{(1-w_{L2.5})w_{cBPE} + w_{L2.5}w_{cL2.5}}\right) \quad (4)$$

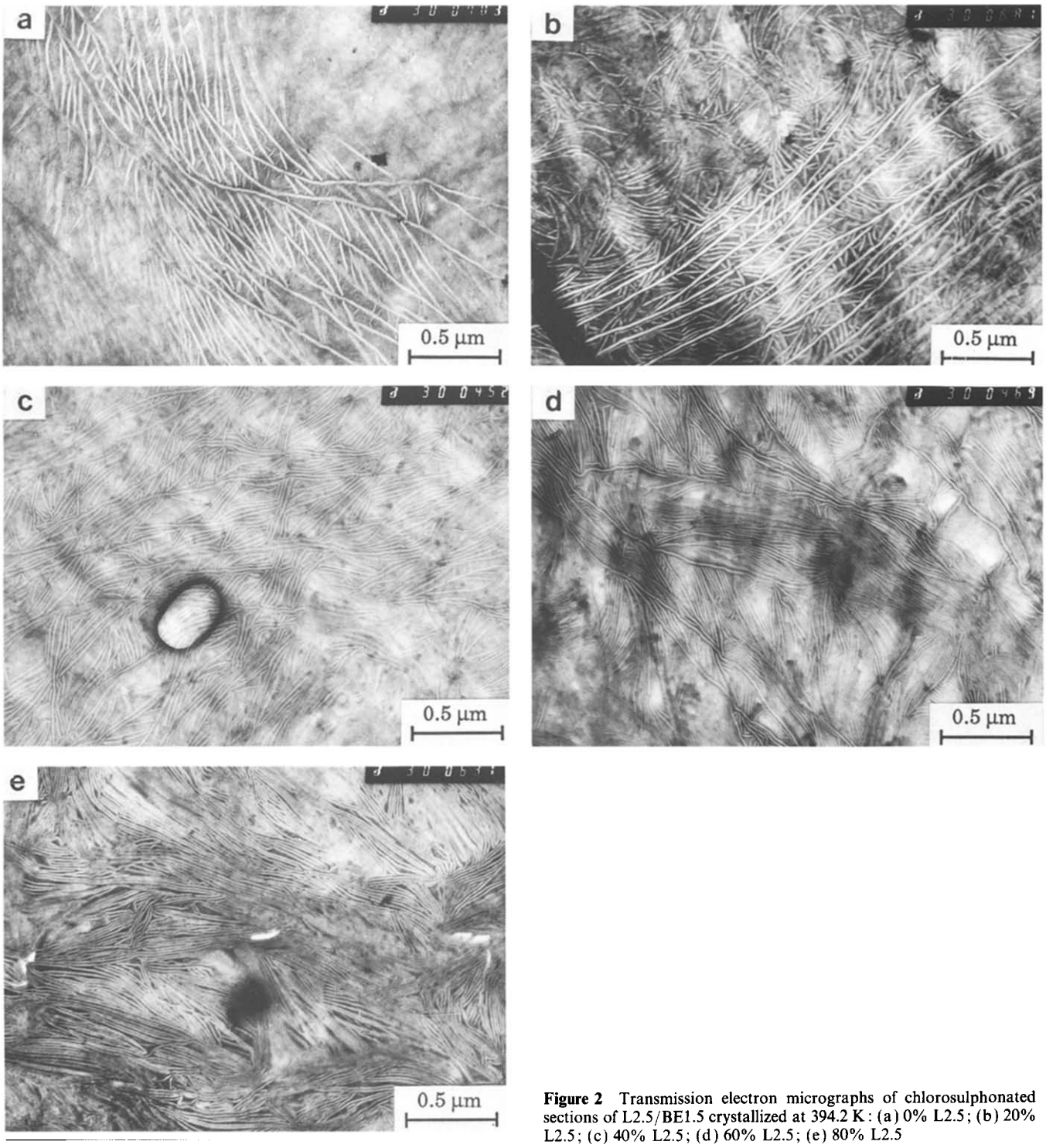

Figure 2 Transmission electron micrographs of chlorosulphonated sections of L2.5/BE1.5 crystallized at 394.2 K: (a) 0% L2.5; (b) 20% L2.5; (c) 40% L2.5; (d) 60% L2.5; (e) 80% L2.5

where N_{e0} is the number of chains crossing (0 0 1) per unit area, θ is the tilt angle (see the data shown in *Figure 14*), w_{cBPE} is the mass crystallinity of the branched polymer, $w_{cL2.5}$ is the mass crystallinity of L2.5, M_w is the mass-average molar mass of L2.5 (2500), ρ_c is the crystalline density at 300 K (equal to 1000 kg m^{-3} (ref. 18)), L_{rep} is the length of the chain segment (equal to $c/2$, which is 0.127 nm[18]), M_{rep} is the molar mass of the repeat unit (equal to 14.1 kg kmol^{-1}) and ρ_a is the amorphous density at 300 K (equal to 855 kg m^{-3} (ref. 18)). Equation (4) can be simplified by inserting these values and by considering that the mass-average amorphous thickness of the pure branched polymer ($\langle L_{a0} \rangle$) is equal to:

$$\langle L_{a0} \rangle = (1 - f) N_{e0} (\cos \theta_{BPE}) V_0 \quad (5)$$

By combining equations (4) and (5), the following equation is obtained:

$$\langle L_a \rangle (\text{nm}) = \frac{\cos \theta}{\cos \theta_{BPE}} \langle L_{a0} \rangle \times \left(\frac{(1 - w_{L2.5}) w_{cBPE}}{(1 - w_{L2.5}) w_{cBPE} + w_{L2.5} w_{cL2.5}} \right) + \left(\frac{2.63 (\cos \theta) w_{L2.5} w_{cL2.5}}{(1 - w_{L2.5}) w_{cBPE} + w_{L2.5} w_{cL2.5}} \right) \quad (6)$$

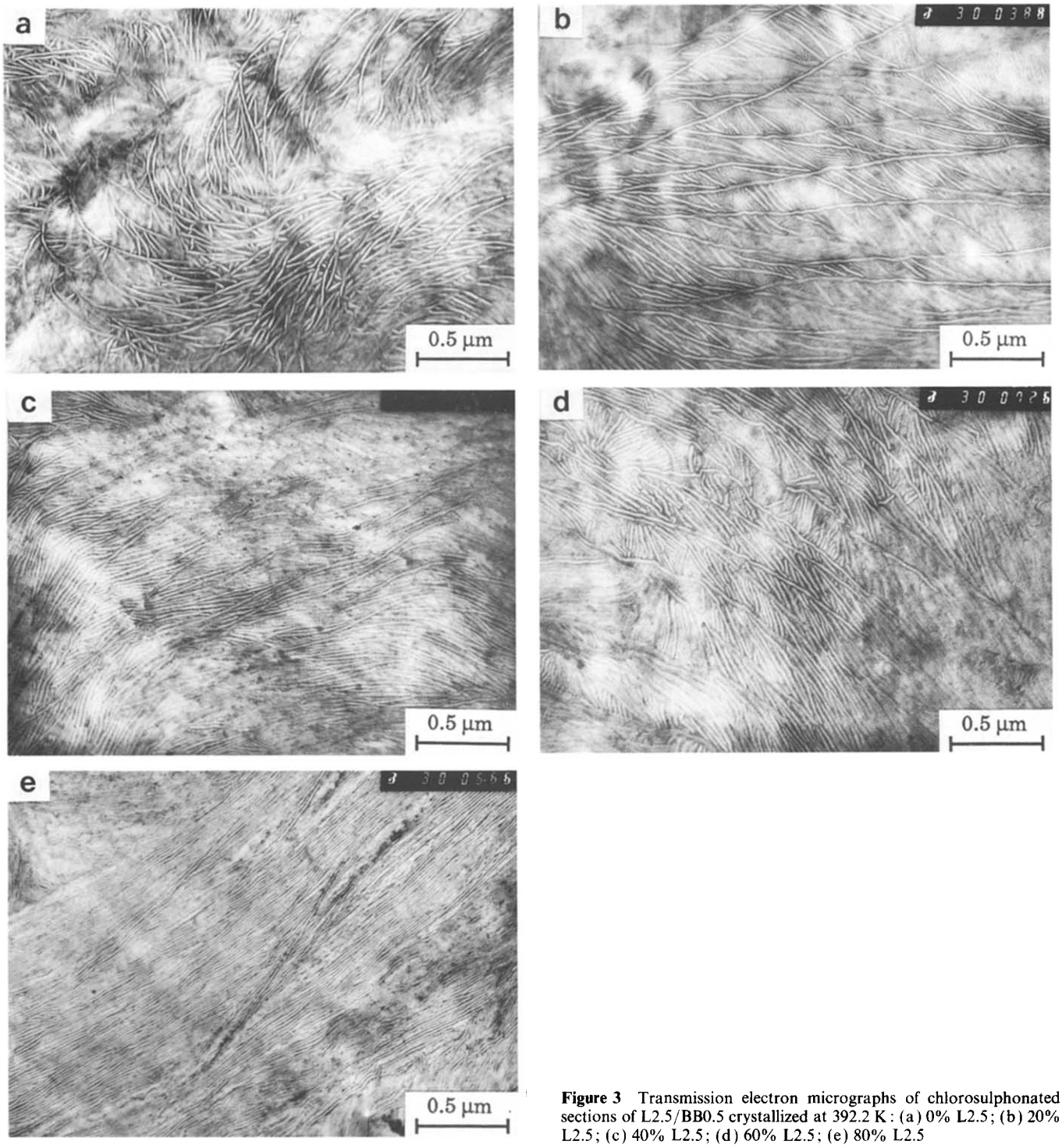

Figure 3 Transmission electron micrographs of chlorosulphonated sections of L2.5/BB0.5 crystallized at 392.2 K: (a) 0% L2.5; (b) 20% L2.5; (c) 40% L2.5; (d) 60% L2.5; (e) 80% L2.5

The blends of L2.5 and BE1.5 exhibit amorphous thickness data in good agreement with the values predicted by the model except for the blend with 80% L2.5. The significantly higher recorded average amorphous thickness for this blend can be explained by partial segregation of L2.5, which in fact is consistent with the data shown in *Figures 6* and *7*. The blends of L2.5 and BB0.5 display a more pronounced deviation from the values predicted by the model. This is also true of blends with a low content of L2.5, which again is consistent with the data presented in *Figures 6* and *7* and can be explained by partial segregation of L2.5. The average amorphous thickness measured for the blend with 80% of L2.5 crystallized at 396.2 K is clearly too low to be consistent with the data shown in *Figure 7*, indicating pronounced segregation of L2.5.

Two questions arise in the analysis of the crystal thickness data: (1) Do bimodal melting-point distributions appear as bimodal crystal thickness distributions? (2) Are the crystal thickness values determined by TEM on the chlorosulphonated sections correct?

The crystal thickness data are presented as mass-average values in *Table 3* and as full distributions in *Figures 11* and *12*. In the blends of L2.5 and BB0.5, the mass-average crystal thickness decreases markedly with increasing content of L2.5 irrespective of crystallization temperature. This is consistent with the data obtained by d.s.c.: the relative size of the low-temperature melting

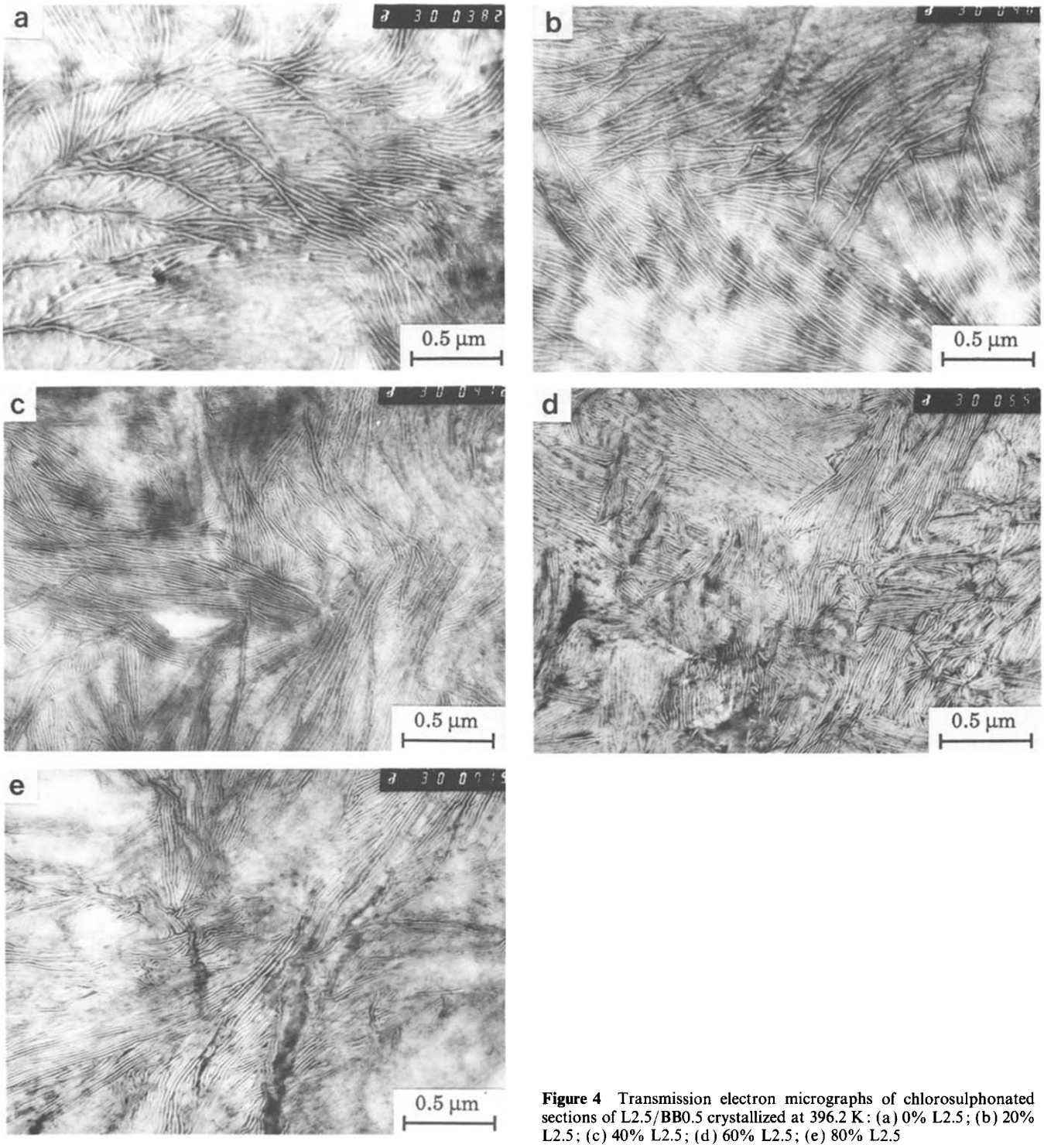

Figure 4 Transmission electron micrographs of chlorosulphonated sections of L2.5/BB0.5 crystallized at 396.2 K: (a) 0% L2.5; (b) 20% L2.5; (c) 40% L2.5; (d) 60% L2.5; (e) 80% L2.5

peak increases with increasing content of L2.5. The minor effect of crystallization temperature on the mass-average crystal thickness of these blends can be explained by the fact that most of the samples that nominally crystallize at 396.2 K crystallized at much lower temperatures during the cooling phase. For the blends of L2.5 and BE1.5 the systematic variations in mass-average crystal thickness are small; an increase of 10–20% over the composition range is recorded (*Table 3*).

The crystal thickness distributions shown in *Figure 11* are selected for comparison with melting thermograms (cf. *Table 1*). The pure BB0.5 exhibits a large high-temperature peak at 407.2 K, constituting 70% of the entire melting, and a significantly broader and smaller low-temperature peak at 390.6 K. The crystal thickness distribution of this sample is bimodal. The dominant peak constitutes approximately 70–80% and ranges between 14 and 23 nm with an average value near 17 nm. The tail appearing at low thickness values ranges from 6 to 12 nm with a maximum near 8 nm. The blend with 80% of L2.5 exhibits a low-temperature peak at 397.8 K constituting 90% of the entire melting. This sample exhibits essentially unimodal crystal thickness distribution averaging at 10.9 nm. A weak shoulder appears at 15 nm supposedly corresponding to the weak high-temperature melting peak. The blend with 40% of L2.5 exhibits a significant high-temperature peak (42%, at 405.4 K) and an even more sizeable low-temperature peak (58%, at

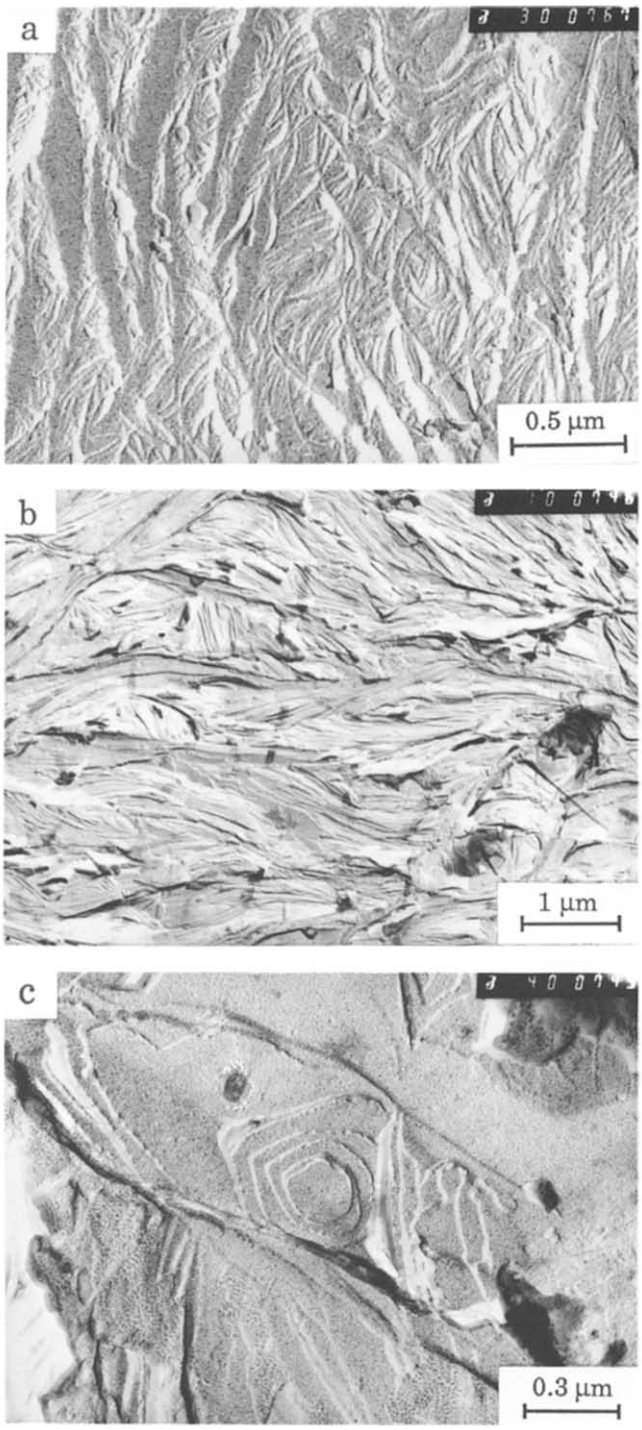

Figure 5 Transmission electron micrographs of samples treated with permanganic acid: (a) L2.5/BE1.5 (0.2/0.8), crystallized at 394.2 K; (b) and (c) L2.5/BE1.5 (0.80/0.20), crystallized at 387.2 K

396.5 K); and accordingly also a pronounced bimodal crystal thickness distribution peaking at 15 nm and 12 nm (*Figure 11*).

Figure 12a shows histograms for L2.5/BE1.5 0.20/0.80 and 0.60/0.40, both crystallized at 387.2 K, and, despite a pronounced bimodal melting peaking at temperatures of 388.7–389.3 K and 399.9–400.4 K, the crystal thickness distributions are not bimodal. However, the 0.20/0.80 sample with a more dominant low-temperature melting peak exhibits a crystal thickness distribution skewed towards the low thickness side. *Figure 12b* shows

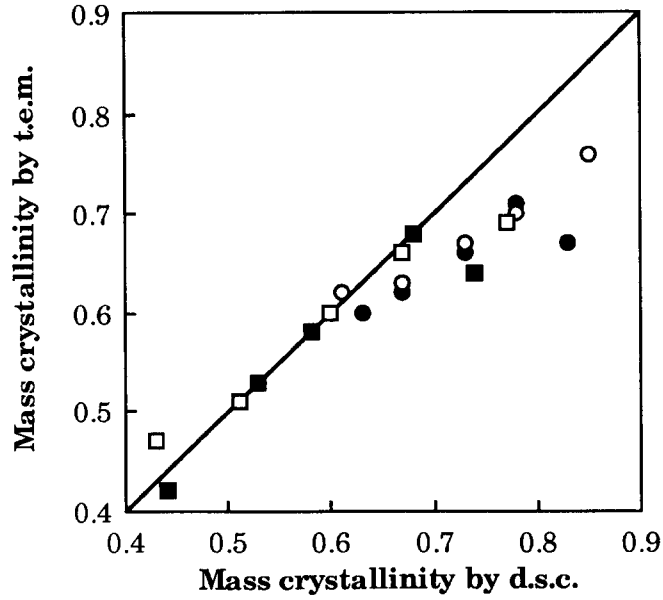

Figure 6 Mass crystallinity obtained by TEM plotted *versus* mass crystallinity by d.s.c. according to equations (2) and (1), respectively, for the following samples: (●) L2.5/BB0.5, 392.2 K; (○) L2.5/BB0.5, 396.2 K; (■) L2.5/BE1.5, 387.2 K; (□) L2.5/BE1.5, 394.2 K

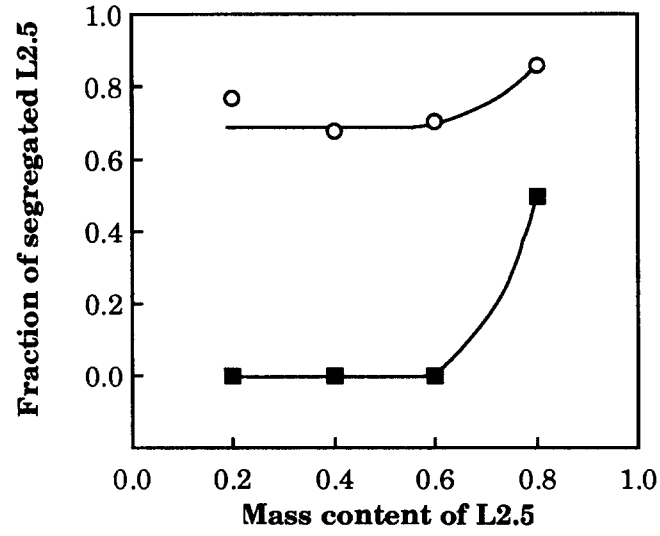

Figure 7 Fraction of L2.5 segregated (from equation (3)) plotted *versus* content of L2.5 for L2.5/BB0.5, 396.2 K (○) and L2.5/BE1.5, 387.2 K (■)

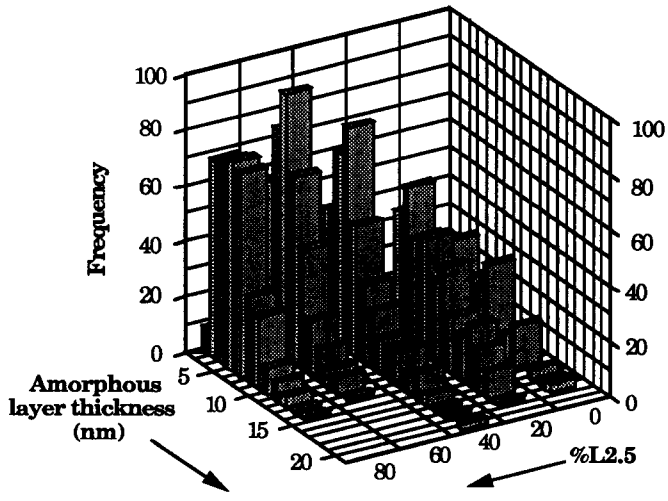

Figure 8 Histograms showing the distribution in amorphous layer thickness for blends of L2.5 and BB0.5 crystallized at 392.2 K

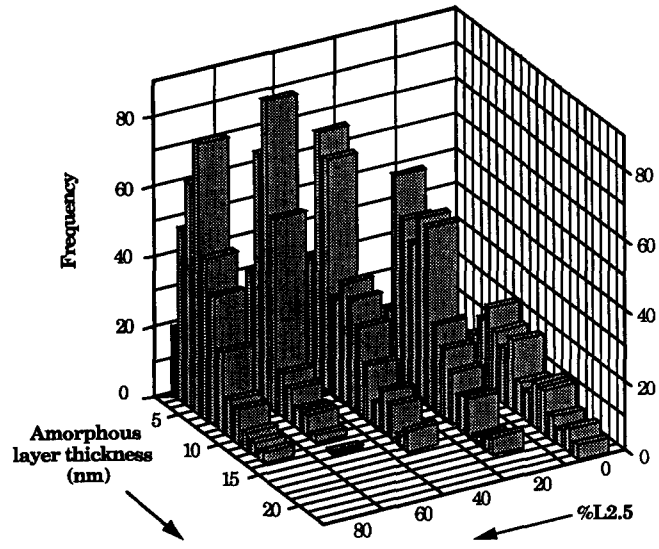

Figure 9 Histograms showing the distribution in amorphous layer thickness for blends L2.5 and BE1.5 crystallized at 394.2 K

Table 3 Average crystal thickness data

Sample	$w_{L2.5}$[a]	T_c (K)	$\langle L_c \rangle$ (nm)[b]
L2.5/BB0.5	0	392.2	13.4
	0.2		15.3
	0.4		13.6
	0.6		13.2
	0.8		11.4
L2.5/BB0.5	0	396.2	15.5
	0.2		15.5
	0.4		13.5
	0.6		13.6
	0.8		10.9
L2.5/BE1.5	0	387.2	9.6
	0.2		11.2
	0.4		11.0
	0.6		12.0
	0.8		11.4
L2.5/BE1.5	0	394.2	11.2
	0.2		10.0
	0.4		11.3
	0.6		11.7
	0.8		13.1

[a]Mass content of linear component (L2.5)
[b]Mass-average crystal thickness

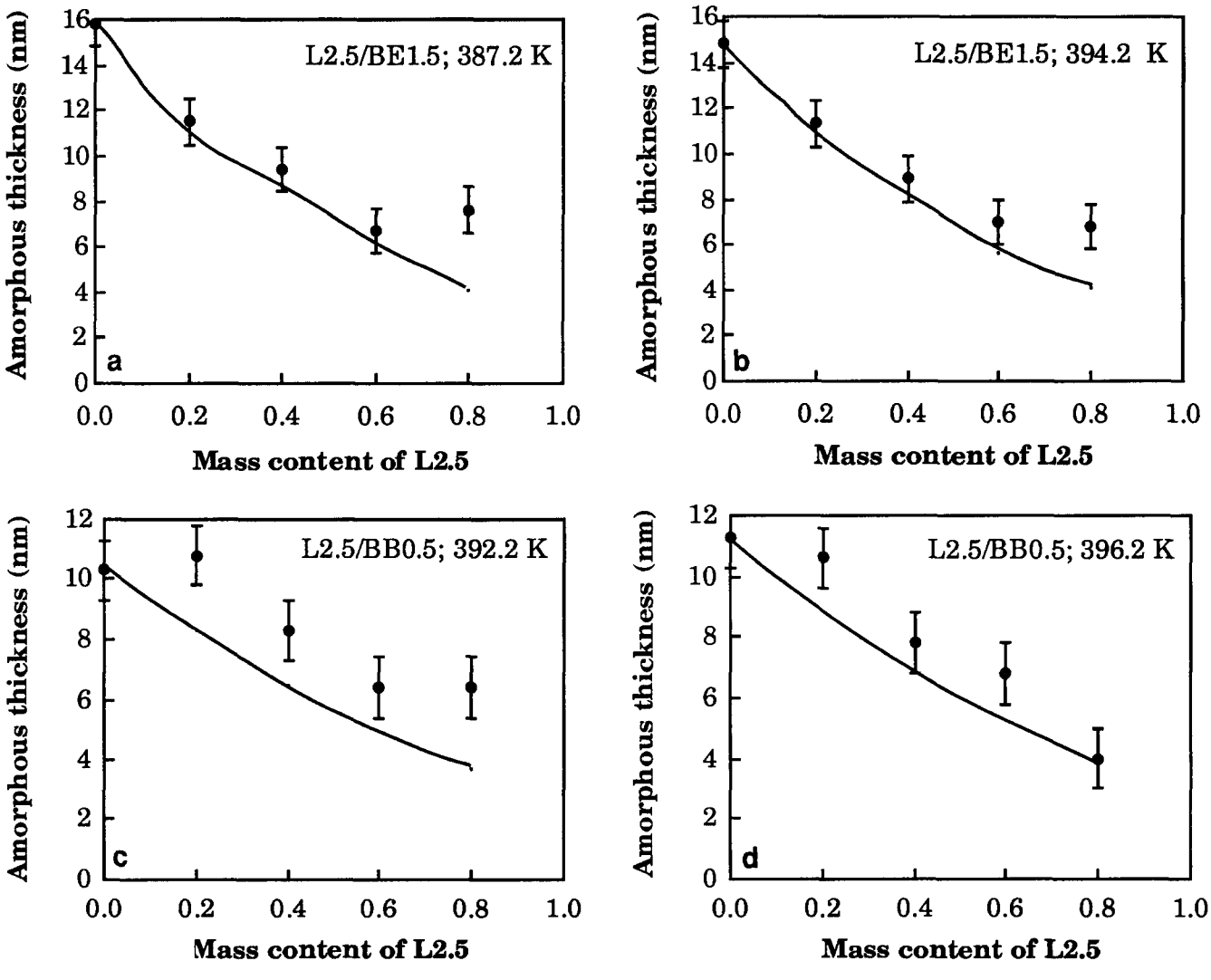

Figure 10 Mass-average thickness of amorphous interlayer ($\langle L_a \rangle$) plotted as a function of mass content of L2.5. The full curves are obtained from model calculations according to equation (5): (a) L2.5/BE1.5, crystallized at 387.2 K; (b) L2.5/BE1.5, crystallized at 394.2 K; (c) L2.5/BB0.5, crystallized at 392.2 K; (d) L2.5/BB0.5, crystallized at 396.2 K

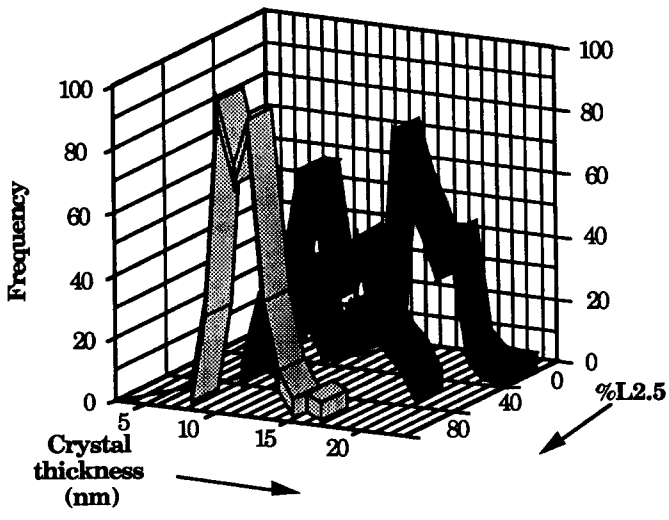

Figure 11 Crystal thickness distribution for three blends of L2.5 and BB0.5 crystallized at 396.2 K

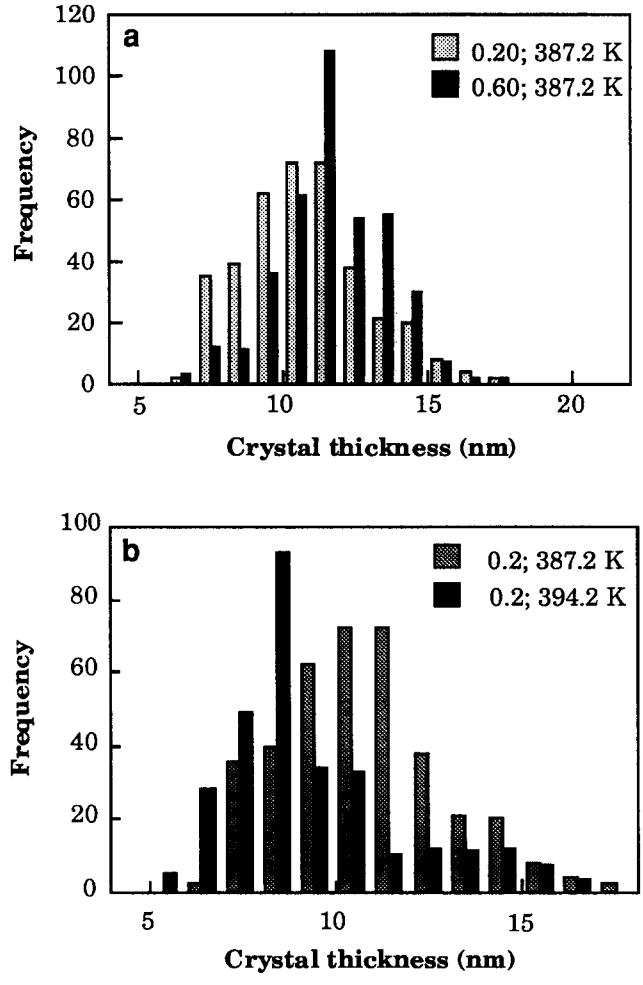

Figure 12 Crystal thickness distribution for blends based on L2.5 and BE1.5: (a) blends consisting of 20 and 60% of L2.5 crystallized at 387.2 K; (b) blend consisting of 20% of L2.5 crystallized at 387.2 and 394.2 K respectively

the effect of crystallization temperature on the crystal thickness distribution. The sample crystallized at 394.2 K exhibits a bimodal distribution with a pronounced low thickness maximum near 10 nm and a weaker and broader high thickness maximum near 15 nm. The melting behaviour of this sample is also bimodal with the major melting peak at 392.4 K and a weaker melting peak constituting 26% of the entire melting at 404.3 K.

TEM has obviously the power to resolve double crystal thickness distributions in some cases, but not always. In the latter case, there seems to be more of a broadening than two separate peaks. Voigt-Martin and Mandelkern[19] compared crystal thickness data by TEM (chlorosulphonated thin sections), Raman spectroscopy and small-angle X-ray scattering (SAXS) on a number of linear PE samples. A sample with a narrow thickness distribution, an average crystal thickness of 21.5 nm and a distribution ranging from 10 to 30 nm, obtained by crystallization at relatively low temperatures, exhibited perfect agreement in crystal thickness data by TEM Raman spectroscopy and SAXS[19]. In samples exhibiting pronounced bimodal distributions or very broad distributions in crystal thickness, TEM clearly underestimated the thicker crystals. In one of the samples, having a bimodal distribution with maximum values at 10 and 15 nm, TEM over-emphasized the thinner crystals. Both populations appeared in the histograms but with incorrect weights[19]. Another sample, which was crystallized at 403 K, exhibited a very broad crystal thickness distribution with maxima at 10, 29, 36 and 40 nm. The 10, 29 and 36 nm crystals were revealed by TEM but with different weightings. The 40 nm crystals on the other hand were only detected by Raman spectroscopy and not by TEM[19]. The crystal thickness data presented in this paper are in general agreement with the extensive data published by Voigt-Martin and Mandelkern[19]. In the following (*Figure 13*) it is shown that the agreement between the melting-point data and the maxima in the crystal thickness distribution data is good. The variations in crystal thickness in the studied samples are not particularly broad and the maximum crystal thickness recorded is less than 25 nm, which according to Voigt-Martin and Mandelkern[19] should be revealed by TEM.

The melting-point data and crystal thickness data should be compared via the Thomson–Gibbs equation:

$$L_c = \frac{2\sigma T_m^\circ}{\Delta h \rho_c (T_m^\circ - T_m)} \tag{7}$$

where σ is the fold-surface free energy, T_m° is the equilibrium melting point for an infinitely thick crystal, Δh is the heat of fusion, ρ_c is the crystal phase density and T_m is the melting point of the crystal of thickness L_c. From equation (7), the derivative of L_c with respect to T_m can be obtained:

$$\frac{\partial L_c}{\partial T_m} = \frac{2\sigma T_m^\circ}{\Delta h \rho_c (T_m^\circ - T_m)^2} \tag{8}$$

Thus, the ability of TEM to resolve double melting peaks increases with increasing melting point, which explains why the bimodal melting of the blends based on L2.5 and BB0.5 is revealed and why that is not universally so for the blends of L2.5 and BE1.5.

In *Figure 13*, a comparison is made between the melting-point data (*Table 1*) and the average crystal thickness data obtained by TEM (chlorosulphonated sections). The melting-point data are corrected for thermal lag between sample pan and sample holder[20] and also for crystal thickening and possible superheating[21]. A linear relationship is established between

the melting point and the reciprocal crystal thickness. The intercept, 420.8 K, is 2.7 K higher than the equilibrium melting point reported[21]. The slope according to the Thomson–Gibbs equation is equal to $-2\sigma T_m^\circ/\Delta h\rho$. By inserting appropriate values for these parameters, $\sigma = 93$ mJ m^{-2} (ref. 22), $T_m^\circ = 418.1$ K (ref. 22), $\Delta h = 293$ kJ kg^{-1} (ref. 11), $\rho_c = 1000$ kg m^{-3} (ref. 18), the slope is determined to be -2.65×10^{-7} K m, which is very close indeed to the value obtained here: -2.68×10^{-7} K m.

Another important question that must be dealt with concerns the thickness of the crystals with respect to the length of the molecules in L2.5. The average molecules, $M = 2500$, give rise to a crystal with a thickness of 17.5 nm assuming 30° tilt angle and 90% mass crystallinity. Thinner and thicker crystals can be accounted for by considering the molar-mass distribution of L2.5 and most probably also by assuming that the chains may be once folded. The crystal thickness distributions obtained by TEM are in this range.

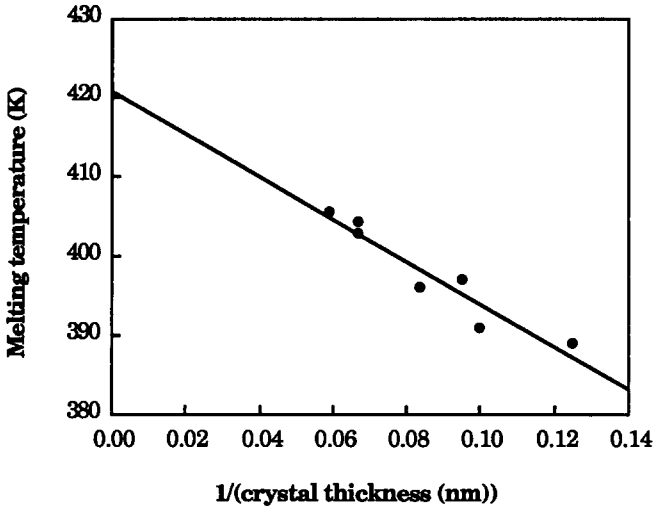

Figure 13 Comparison of melting point (d.s.c.) data and average crystal thickness data by TEM in a Thomson–Gibbs plot; the regression line is given by equation $y = 420.81 - 267.96x$, $r^2 = 0.917$

Most of the blends studied here displayed occasional roof-shaped lamellae. We must stress that this lamellar feature is only occasional. The angle between both sides of the roof is called the apex angle. Previous reports[23–25] have shown that the apex angle measured in chlorosulphonated thin sections can be explained as a combination of (h 0 l) crystallographic planes. It is thus assumed that the roof gable corresponds to [0 1 0][17]. The knowledge of the (h 0 l) crystallographic planes leads to an estimation of the molecular tilt with respect to the lamellar surface normal.

A relatively common case where one side of the roof appeared blurred was not included in the numerical analyses. The number of counted roof-shaped lamellae is therefore relatively small and a proper statistical analysis cannot be performed. However, some trends in the data can be observed. Neither of the pure branched polymers (BE1.5 and BB0.5) exhibit any roof-shaped lamellae. Curved, S- or C-shaped lamellae occur frequently in these samples. For the blends of L2.5 and BE1.5, crystallized at both 387.2 and 394.2 K, there is a significant increase in frequency of observed roof structures with increasing content of L2.5 up to 60% of L2.5, above which the frequency remains constant. The blends based on L2.5 and BB0.5 exhibit fewer roof structures and also a different compositional dependence at the highest crystallization temperature (396.2 K). The blend consisting of 80% of L2.5 displays essentially no roof-shaped lamellae. It is worth noting that almost all crystallization in this sample occurs during the subsequent cooling phase.

The apex angle distributions are generally very broad, and it has been possible to identify specific crystallographic fold planes on both sides of the roof gable. *Table 4* presents a summary of all roof structures observed in one of the blends. The situation in which there are different crystallographic planes on the two sides of the gable is undoubtedly the most common case.

Figure 14 presents a summary of roof structures expressed in terms of average chain tilt angle. There is a considerable scatter in the data of L2.5/BB0.5, primarily due to the low number of measured apex angles. There

Table 4 Features of roof structures observed in L2.5/BE1.5 (0.8/0.2) crystallized at 394.2 K

Measured apex angle (deg)	Crystallographic planes; incl. apex angle[a]	Chain tilt[b] (deg)	Frequency
106	(3 0 2), (3 0 1); 107°	27; 46	1
111	(2 0 1); 111°	34	2
116	(1 0 1), (3 0 1); 115°	19; 46	1
117	(1 0 2), (4 0 1); 116°	10; 54	1
118	(3 0 2), (2 0 1); 118°	27; 34	2
125	(3 0 1), (1 0 2); 124.5°	46; 10	6
127	(3 0 2); 126°	27	1
127	(2 0 1), (1 0 1); 127°	34; 19	4
134	(3 0 2), (1 0 1); 134°	27; 19	3
137	(1 0 2), (2 0 1); 136°	10; 34	4
143	(3 0 2), (1 0 2); 143°	27; 10	3
145	(3 0 1), (1 0 2); 144°	46; 10	6
145	(0 0 1), (2 0 1); 145.5°	0; 34	3
149	(1 0 1), (1 0 2); 151°	19; 10	2
160	(1 0 2); 160.5°	10	1

[a]The apex angle given exactly by the crystallographic planes
[b]Chain tilt refers to the angle between the chain axis and the normal of the lamella

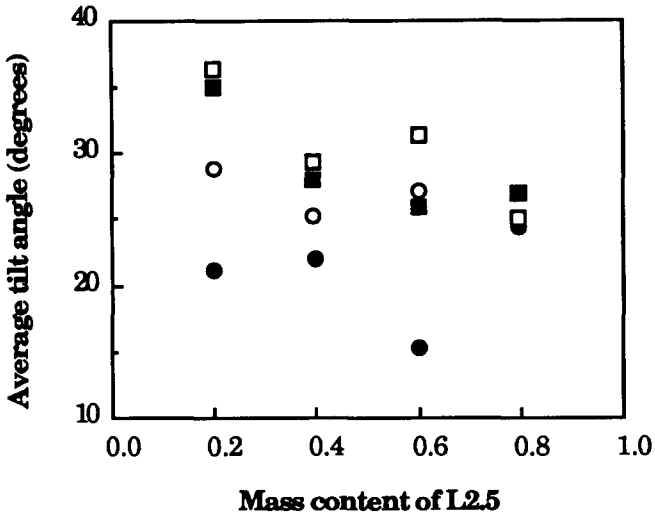

Figure 14 Average chain tilt angle (determined from apex angle in roof-shaped lamellae) plotted as a function of mass content of L2.5: (●) L2.5/BB0.5, 392.2 K; (○) L2.5/BB0.5, 396.2 K; (■) L2.5/BE1.5, 387.2 K; (□) L2.5/BE1.5, 394.2 K

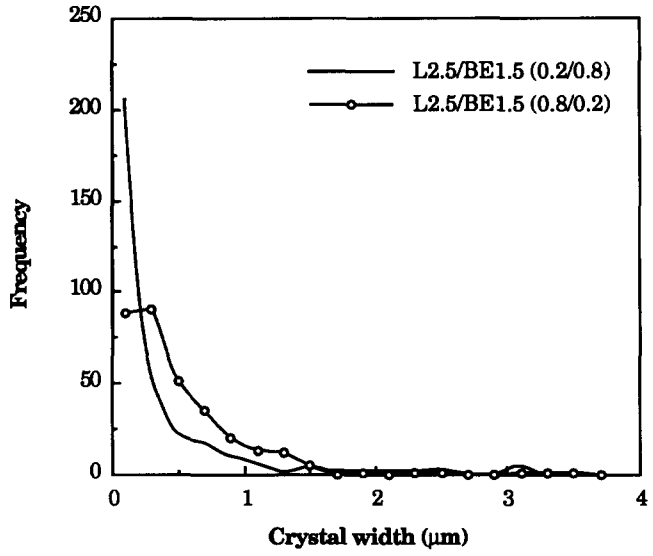

Figure 15 Distribution in crystal lamellar width for two samples crystallized at 394.2 K: L2.5/BE1.5 (20/80) and L2.5/BE1.5 (80/20)

is no clear trend in chain tilt angle data for these blends, neither with crystallization temperature, nor with composition. The reduction in average chain tilt angle with increasing content of L2.5 is characteristic of the blends based on L2.5 and BE1.5. The falling trend is similar for samples crystallized at both temperatures (387.2 and 394.2 K).

TEM of chlorosulphonated sections reveals dominantly the crystal lamellae as viewed along [0 1 0]. The crystal growth direction is therefore primarily towards the observer. It is thus possible to determine the lamellar width directly from the electron micrographs. A serious problem is that lamellar contrast is obtained only when the fold surface is almost parallel to the electron beam. The lamellar width can thus only be determined on crystals that appear with sharp boundaries along their entire width, and hence this method underestimates the widest crystals.

Figure 15 presents for comparison the distribution of two samples (L2.5/BE1.5) with different compositions. The blend with 80% of L2.5 exhibits wider crystals than the blend consisting of 20% of L2.5. The average values for these and the other samples are presented in *Table 5*. The only established trend in these data is that the average crystal width increases with increasing content of L2.5.

CONCLUSIONS

Binary blends based on low-molar-mass linear polyethylene (L2.5) and two higher-molar-mass branched polyethylenes have been examined with regard to their morphology as revealed by transmission electron microscopy, polarized light microscopy and differential scanning calorimetry. The two branched polymers contained 1.5 mol% of ethyl groups (BE1.5) or 0.5 mol% of butyl groups (BB0.5).

All the thermal treatments consisted first of a period at 440 K at which the blends were held in the molten state, secondly a constant-temperature phase during which a certain fraction crystallized, and thirdly a rapid cooling phase during which the remaining crystallization occurred. The fact that different molecular species crystallize at different temperatures implies that segregation occurs. It is important here to note that neither of the components was truly monodisperse. They contained species of different chain lengths, and in the branched polymers the branches were randomly positioned on the chains. Thus, the pure components exhibit segregation on crystallization. The relevant questions here are: (1) Are the linear and branched components crystallizing separately or together under the isothermal conditions? (2) Is separate or co-crystallization occurring during the rapid cooling? It is possible to add an extra question concerning the possibility of liquid–liquid segregation in the molten state.

The evidence obtained by the different methods used in this study is as follows.

Table 5 Average crystal width data

Sample	$w_{L2.5}$[a]	T_c (K)[b]	$\langle L_{wc} \rangle$ (μm)[c]
L2.5/BB0.5	0	392.2	0.17
	0.2		0.24
	0.4		0.28
	0.6		0.34
	0.8		0.44
L2.5/BB0.5	0	396.2	0.22
	0.2		0.24
	0.4		0.27
	0.6		0.40
	0.8		0.47
L2.5/BE1.5	0	387.2	0.19
	0.2		0.25
	0.4		0.26
	0.6		0.35
	0.8		0.50
L2.5/BE1.5	0	394.2	0.30
	0.2		0.36
	0.4		0.44
	0.6		0.47
	0.8		0.49

[a] Mass content of linear component (L2.5)
[b] Crystallization temperature
[c] Number-average crystal width based on 300–400 measurements

D.s.c. revealed either two or three melting peaks. The latter case is indicative of the formation of two different crystallite populations, i.e. segregation under the isothermal conditions. The presence of one high-temperature melting peak with a relative size approaching zero when the content of one of the components approaches zero is indicative of separate crystallization of this component. However, the presence of only two melting peaks is necessary but not sufficient experimental evidence for co-crystallization within each of the two different thermal phases. It is possible to have two different crystallite populations with overlapping melting peaks[26].

The supermolecular structure revealed by polarized light microscopy gave no conclusive evidence in favour of any of the possibilities. The diffusion distance is short in polymers and segregation occurs therefore only on a microscale, which may not be revealed by polarized light microscopy. Segregation was not revealed by polarized light microscopy and this confirmed that mixing prior to the thermal treatment was properly performed.

TEM, which measures the amorphous thickness, gave direct evidence about the state of mixing of the two components. The selection of constituents, one of them forming extended-chain or once-folded-chain crystals with almost no amorphous thickness and the branched polymers with an appreciable, 10–15 nm thick amorphous phase, was ideal for these studies. It was also possible to estimate the perfection of the mixing by comparing the observed average value for the amorphous thickness with that obtained by a simple model calculation. TEM provided other possibilities for obtaining information about the mixing. Crystallinity assessments by d.s.c. and by TEM correspond if mixing is intimate. Isolated domains of high-crystallinity, low-molar-mass component are not revealed by TEM and hence any systematic deviation between the two is due to segregation. The shape of the crystal lamellae clearly reflects the local composition; the branched polymers exhibit curved lamellae whereas the low-molar-mass linear polyethylene displays wide and straight crystals. Co-crystals exhibit intermediate morphologies.

For the binary blends based on L2.5 and BB0.5 crystallized at 396.2 K, separate crystallization of the high-melting-point species of BB0.5 was conclusively shown by d.s.c. The crystallization in the cooling phase gave crystallites with unimodal melting. The reduction in the average amorphous thickness with increasing overall content of L2.5 together with the general change in morphology from curved, S-shaped to straight lamellae indicated partial co-crystallization of the linear and branched polymers. Comparison of d.s.c. and TEM crystallinities and comparison of the average amorphous phase thickness with predicted values from model calculations indicate that an appreciable fraction of L2.5 is segregated: approximately 70% in samples containing 20–60% of L2.5 and 85% in the samples with 80% of L2.5. The blends crystallized at 392.2 K exhibit a very similar behaviour, the only difference being that some co-crystallization of linear and branched polymers also occurs in the isothermal phase. For samples with 40% of L2.5 or less, unimodal melting occurs, and for samples with a higher content of L2.5, bimodal melting is evident, indicating at least partial segregation under the isothermal conditions.

The blends based on L2.5 and BE1.5, which have crystallized at 394.2 K, showed first a separate crystallization of the most perfect (30%) chains of the branched polymer and then during cooling almost complete co-crystallization of the linear and branched polymers. The sample with 80% of L2.5 exhibited partial segregation of L2.5 involving approximately 50% of L2.5. Similar results were obtained for L2.5/BE1.5 crystallized at 387.2 K, the only important difference being that most of the crystallization in this case occurred under the isothermal conditions.

ACKNOWLEDGEMENTS

This work has been sponsored by the Swedish Board for Technical Development (STU), grant 89-02294P, the National Energy Administration of Sweden (STEV), grant 656109-1, and the Swedish Plastics Federation. The authors thank Neste Polyeten AB, Sweden, for the PE grades and Dr I. Iragorri for experimental assistance.

REFERENCES

1 Clampitt, B. H. *J. Polym. Sci.* 1965, **3**, 671
2 Datta, N. K. and Birley, A. W. *Plast. Rubb. Process. Appl.* 1982, **2**, 237
3 Kyu, T., Hu, S.-R. and Stein, R. S. *J. Polym. Sci., Polym. Phys. Edn* 1987, **25**, 89
4 Hu, S.-R., Kyu, T. and Stein, R. S. *J. Polym. Sci., Polym. Phys. Edn* 1987, **25**, 71
5 Edward, G. H. *Br. Polym. J.* 1986, **18**, 88
6 Norton, D. R. and Keller, A. *J. Mater. Sci.* 1984, **19**, 447
7 Rego Lopez, J. M. and Gedde, U. W. *Polymer* 1989, **30**, 22
8 Conde Braña, M. T., Iragorri Sainz, J. I., Terselius, B. and Gedde, U. W. *Polymer* 1989, **30**, 410
9 Iragorri Sainz, J. I., Rego Lopez, J. M., Katime, I., Conde Braña, M. T. and Gedde, U. W. *Polymer* 1992, **33**, 461
10 Gray, A. P. *Thermochim. Acta* 1970, **1**, 563
11 Wunderlich, B. in 'Macromolecular Physics', Vol. 3; 'Crystal Melting', Academic Press, New York, 1980
12 Hoffman, J. D., Frolen, L. J., Ross, G. S. and Lauritzen, Jr, J. I. *J. Res. Natl Bur. Std (A)* 1975, **79**, 671
13 Wunderlich, B. and Baur, H. *Adv. Polym. Sci.* 1970, **7**, 151
14 Kanig, G. *Colloid Polym. Sci.* 1977, **255**, 1005
15 Olley, R. H. and Bassett, D. C. *Polymer* 1982, **23**, 1707
16 Grubb, D. T. and Keller, A. *J. Polym. Sci., Polym. Phys. Edn* 1980, **18**, 207
17 Bassett, D. C. and Hodge, A. M. *Proc. R. Soc. Lond. (A)* 1978, **359**, 121
18 Wunderlich, B. in 'Macromolecular Physics', Vol. 1, 'Crystal Structure, Morphology and Defects', Academic Press, New York, 1973
19 Voigt-Martin, I. G. and Mandelkern, L. *J. Polym. Sci., Polym. Phys. Edn* 1989, **27**, 967
20 *Thermal Analysis Newsletters*, No. 5, Perkin–Elmer Corporation, Norwalk, Connecticut
21 Gedde, U. W. and Jansson, J.-F. *Polymer* 1983, **24**, 1521
22 Hoffman, J. D., Frolen, L. J., Ross, G. S. and Lauritzen, Jr, J. I. *J. Res. Natl Bur. Std (A)* 1975, **79**, 671
23 Voigt-Martin, I. G., Fisher, E. W. and Mandelkern, L. *J. Polym. Sci., Polym. Phys. Edn* 1980, **18**, 2347
24 Voigt-Martin, I. G. and Mandelkern, L. *J. Polym. Sci., Polym. Phys. Edn* 1981, **19**, 1769
25 Stack, G. M., Mandelkern, L. and Voigt-Martin, I. G. *Macromolecules* 1984, **17**, 321
26 Rego Lopez, J. M., Conde Braña, M. T., Terselius, B. and Gedde, U. W. *Polymer* 1988, **29**, 1045